Observation of Filamentous Nanostructures in Organic-Inorganic Composite Thin Films Deposited by Co-Evaporation

Daniela Donhauser, Martin Pfannmöller, Levin Dieterle, Katrin Schultheiß, Rasmus R. Schröder, Wolfgang Kowalsky, and Michael Kröger*

Nanostructures are important for a wide area of applications, but are very often difficult to fabricate. A novel and basic approach for controlled nanofilament growth in an organic/inorganic composite material is demonstrated. Thin films of MoO_3-doped 4′-bis(*N*-carbazolyl)-1,1′-biphenyl are grown via vacuum sublimation and analyzed using advanced electron microscopy and spectroscopy techniques. Using electron spectroscopic imaging in the core-loss and low-loss regime, MoO_3 agglomerations are identified for different doping concentrations. A 3D reconstruction of the thin film yielded by electron tomography reveals a filamentous structure of MoO_3 within the organic matrix. These filaments are preferentially oriented along the growth direction and are only a few nanometers in diameter. Furthermore, control of the filament growth is possible by changing the substrate temperature because for composites grown on substrates cooled to 120 K MoO_3 agglomeration cannot be detected.

1. Introduction

Understanding and control of the nanostructure within composite materials show great potential for future applications fields such as targeted drug delivery and tissue engineering,[1] plasmonics,[2] resistive memory switching,[3,4] third generation solar cells[5] or efficient thermoelectric energy conversion.[6,7] Controlled nanomorphologies have been obtained, e.g., via microemulsion-based reactions,[8,9] chemical vapor deposition,[10] directly patterned, respectively templated growth,[11] and self-assembly or assisted phase separation using defined annealing procedures.[12,13] Using these techniques, nanometer-sized low-dimensional structures such as nanodots or nanowires have been realized in inorganic/inorganic, inorganic/organic and organic/organic composite materials. For instance, inorganic/inorganic nanocomposite thermoelectric materials can outperform their bulk counterparts, as the interdependency of heat and charge transport can be suppressed.[6] In 1D wires surface phonon scattering, which limits the heat conduction and the figure of merit, *ZT*, drastically increases when the width of the conducting wires becomes smaller than 2 nm.[7] To fully describe nanostructured growth or self-assembly processes and hence to understand the underlying physical principles in nanocomposite materials and devices, structural characterization becomes extremely important. Extensive studies of P3HT/PCBM polymer blend films, an example for organic/organic nanocomposites, showed that a complex relationship between three different phases is responsible for efficient charge separation in so-called bulk-heterojunction solar cells.[13,14]

Here we present a transmission electron microscopy (TEM) study on how the formation of few-nm-wide filaments in an organic/inorganic composite thin film can be controlled using vacuum thermal evaporation. We co-evaporated the transition metal oxide (TMO) MoO_3 with the organic molecular compound 4,4′-bis(*N*-carbazolyl)-1,1′-biphenyl (CBP). Latter is often used as charge transporting material in organic light-emitting diodes.[15–18] It was recently reported that when doping MoO_3 into CBP a greatly enhanced conductivity is measured which was attributed to the strong electron-withdrawing nature of MoO_3 originating from very deep-lying unoccupied states.[19] Despite its favorable electronic structure, doping efficiency, meaning the measured number of free charge carriers compared to the number of incorporated dopant molecules, is much lower than expected when using MoO_3 or other TMOs as dopants.[20,21] Latter conclusion of a low doping efficiency is inferred from the idea, that MoO_3 is homogeneously dispersed in the organic matrix. In the following, we use bright-field transmission electron microscopy, electron spectroscopic imaging (ESI) and electron tomography to investigate the

D. Donhauser, Dr. L. Dieterle, Dr. K. Schultheiß, Prof. W. Kowalsky, Dr. M. Kröger
Institut für Hochfrequenztechnik
Technische Universität Braunschweig
Schleinitzstraße 22, 38106 Braunschweig, Germany
E-mail: daniela.donhauser@ihf.tu-bs.de
D. Donhauser, Dr. L. Dieterle, Dr. K. Schultheiß, Prof. W. Kowalsky, Dr. M. Kröger
InnovationLab GmbH
Speyererstraße 4, 69115 Heidelberg, Germany
M. Pfannmöller, Prof. R. R. Schröder
CellNetworks, BioQuant, Universität Heidelberg
Im Neuenheimer Feld 267, 69115 Heidelberg, Germany

DOI: 10.1002/adfm.201202089

nanostructure of MoO_3 doped into an organic matrix. We show that the concept of homogeneously dispersed MoO_3 is not valid, but MoO_3 nanofilaments of a few nanometer thickness and preferentially oriented perpendicular to the substrate plane dominate. Additionally we confirm that the nanofilament growth can be controlled by substrate temperature. Our results direct towards a novel and very basic approach of generating inorganic/organic composite nanofilaments for potential thin-film device applications.

2. Results and Discussion

2.1. Observation of Dopant Agglomeration Via Bright-Field TEM

We prepared two MoO_3-doped CBP samples with doping concentrations of 10 vol% and 33 vol%. The thin films were deposited via co-evaporation of CBP and MoO_3 (see Experimental Section for more information about the sample preparation). The structure of the thin films was analyzed by Debye electron diffraction. **Figure 1**c shows a zero-loss filtered and contrast inverted Debye diffraction pattern of the sample with 10 vol% doping concentration. The diffuse concentric circles are due to the amorphous nature of MoO_3 and CBP and can also be seen for neat films and other doping concentrations (not shown here).

Figure 1a,b show TEM bright-field microscopy images of these two specimens in plane-view perspective. In both samples dark spots are observed, whose density increases with doping concentration. Power spectral density analysis[22] shown in Figure 1d was used to determine size distributions of the agglomerations. The mean distances between the MoO_3 clusters are 7 nm and 4.3 nm, respectively, as determined from the main peaks at lower frequencies (indicated by solid lines). The feature at higher frequency (dotted line) corresponds to the mean lateral agglomeration size of the clusters, which is 1 nm for both samples, confirming findings of Lee et al.[23] These dark spots, potentially, represent MoO_3 agglomerations, indicating that MoO_3 does not disperse homogenously in the organic matrix.

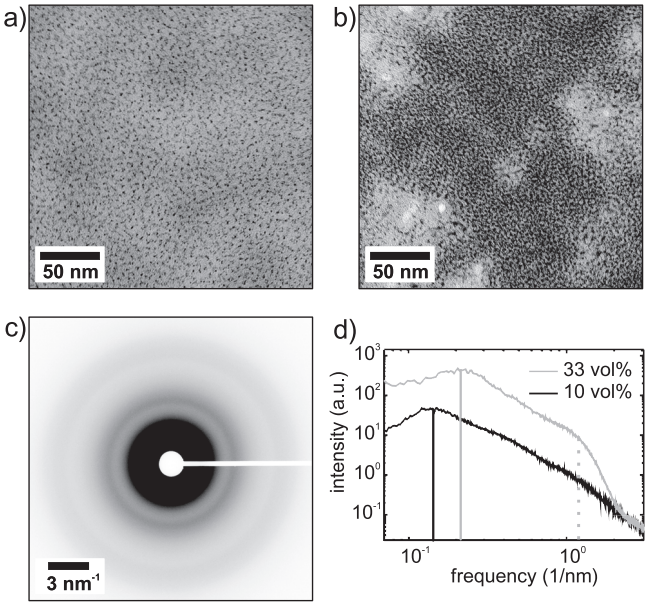

Figure 1. Bright-field images of MoO_3-doped CBP samples with doping concentration of a) 10 vol% and b) 33 vol%. c) Electron diffraction pattern of the sample with 10 vol% doping concentration. d) Calculated power spectral density for both films.

2.2. Material Contrast with TEM Spectroscopy in the Low-Loss and Core-Loss Regime

It can be argued that the contrast in Figure 1a,b can also be due to other effects such as local variations in the morphological structure as, e.g., amorphous and crystalline domains or thickness fluctuations. To resolve this ambiguity and to clearly identify MoO_3 in the thin film, we applied analytical electron microscopy (EELS and ESI), where inelastic scattering processes due to the interaction of the electron beam with the specimen leads to a specific energy loss of the interacting electrons. To gain spectral information on the specimen, electron energy loss spectroscopy (EELS) can be used, where spectral information of the whole transmitted sample area is collected. Using a monochromated beam this measurement technique provides high energy resolution of up to 80 meV at 60 kV incident beam energy. For imaging with chemical contrast electron spectroscopic imaging (ESI) can be applied. Here a series of TEM images at specific loss energies are collected and analyzed to spatially discriminate local chemical distributions.[24,25] ESI is typically applied in two energy regimes: for elemental analysis core-loss spectroscopy is used, where ionization-edges of tightly bound core electrons, with energies characteristic for each element, can be used to differentiate between specific elements. This imaging mode provides chemical contrast and is routinely applied for direct elemental mapping of inorganic samples. However, because of the low ionization cross-section and hence, poor signal-to-noise ratio, longer data collection times and therefore higher beam doses are required. For thin organic films this can cause various disadvantages: i) the long data collection time increases the spatial sample drift during the measurement making it difficult to achieve nanometer-resolution and ii) because of the high electron-dose, beam-damage of the sample can be substantial and can induce distortions of the thin film. To overcome these problems low-loss ESI can be applied. The low-loss energy range is typically assigned to energies between 0 eV and about 60 eV, where electronic and plasmonic excitations occur. Because the cross-sections of these excitations are much higher, shorter data collection times are required and issues due to beam damage and spatial sample drift can be reduced.

2.2.1. Core-Loss Spectroscopy for Direct Elemental Mapping

The oxygen K-edge of MoO_3 at 532 eV[26,27] allows mapping of the local MoO_3-distribution in the CBP matrix, as CBP does not contain any oxygen. Core-loss ESI as well as EELS were performed with low electron doses to ensure that no phase transition occurs.[27] No changes in spectrum shape or peak ratio were observed due to the electron irradiation during data acquisition. Background-corrected EELS-spectra of the oxygen K-edge of

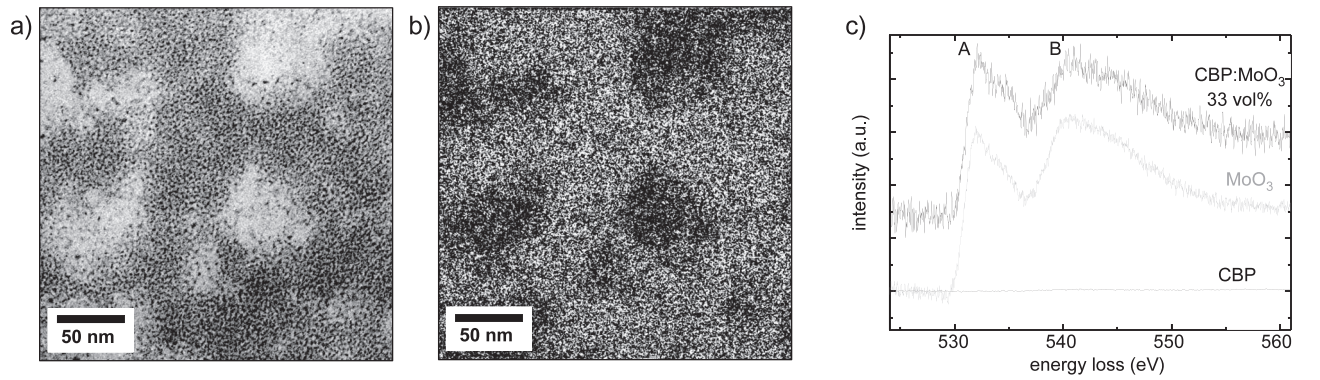

Figure 2. a) Bright-field image of CBP-sample doped with 33 vol% MoO_3. b) Oxygen distribution mapped with the O-K edge (three-window method). c) EELS-spectra of the O-K edge for the doped film and neat CBP and MoO_3 films.

neat films and a 33 vol% MoO_3 doped CBP-film are displayed in **Figure 2**c. These spectra were normalized with respect to the intensity of indicated peak A. The spectrum for neat MoO_3 shows a very distinct energy-loss spectrum with peaks at 532 eV and 541 eV as indicated by markers A and B. The respective spectrum of the MoO_3-doped CBP film shows only little differences in the intensity ratio of peak A and B as compared to the neat film. No fundamental spectral shifts or changes in spectral intensity as expected for different stoichiometry[27] were observed. Therefore we conclude that co-evaporation does not have a significant effect on the MoO_3 stoichiometry. Additionally, the spectrum of the intrinsic CBP film does not show features in this energy range, hence allowing for discrimination of the two materials from ESI. The three-window method[28–30] (using an energy window of 30 eV and pre-edge images at 484 eV and 514 eV) was applied at the O-K ionization edge to study the elemental distribution of oxygen and therewith the distribution of MoO_3. The resulting core-loss map is shown in Figure 2b, where areas of high spectral intensity are assigned to MoO_3 (white) and areas of low spectral intensity to CBP (black). A comparison with the corresponding bright-field image of Figure 2a illustrates that the bright-field correlates very well with the ESI-measurement, i.e., the ESI-measurement shows signal were dark spots appear in the bright-field image and no signal in the bright regions, clarifying that dark spots in the bright-field images can be assigned to MoO_3 agglomerations.

2.2.2. Low-Loss Spectroscopy

Because of the problems mentioned above low loss ESI was applied for the sample with lower MoO_3-content. For measurements in the low-loss regime a stack of ESI images between 3 and 60 eV was acquired in 1 eV steps with a slit aperture of 1 eV to acquire a spectrum for each pixel (see Supporting Information Movie 1). All these spectra were normalized by dividing each pixel intensity value by the integral of the spectrum of the respective pixel to account for thickness variations. Then multivariate statistical analysis was applied, as described in detail previously.[14] Using this technique, even small differences in local spectra can be identified and enables us to classify different materials based on spectral information. From our data (see Supporting Information Figure S1) two individual classes can be identified, one representing CBP and the other one MoO_3. **Figure 3**c shows the experimentally obtained low-loss EELS spectra of the neat films as well as the averaged spectra of the classification from the ESI-data of the sample doped with 10 vol%. As can be seen in the insets of Figure 3c, contrast in the ESI microscopy images is mainly due to an ionization-edge

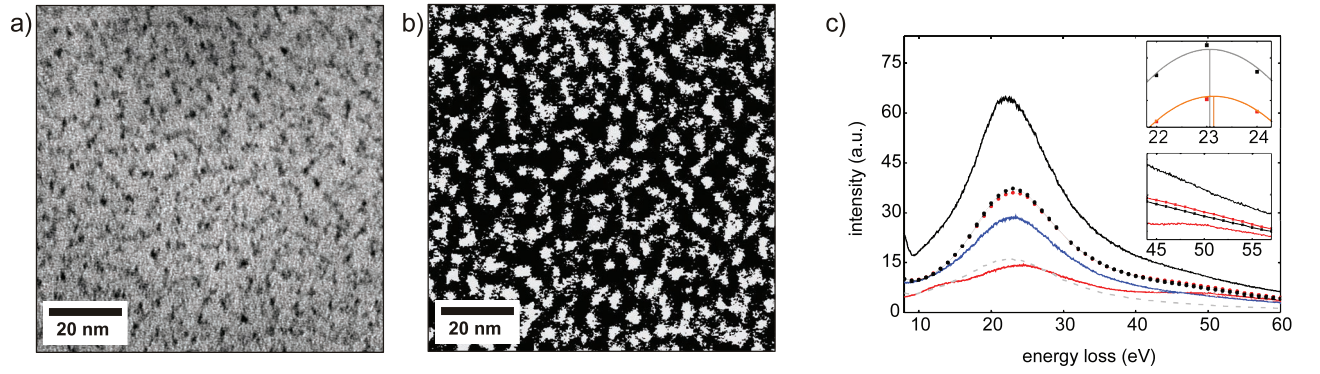

Figure 3. a) Bright-field image of CBP-sample doped with 10 vol%. b) Low-loss ESI classification map where MoO_3 is depicted in white and CBP in black. c) Low-loss EELS-spectra for neat and doped films compared to the characteristic spectra obtained from classification. blue solid: CBP: MoO_3 (10 vol%), red solid: MoO_3 + carbon support film, black solid: CBP + carbon support film, grey dashed: carbon support film, black dotted: spectra obtained from classification for CBP, red dotted: spectra obtained from classification for MoO_3. Inset: grey solid: gaussian fit of MoO_3-plasmon-peak, orange solid: gaussian fit of CBP plasmon-peak.

(Mo-N2, 3) around 50 eV which is characteristic for MoO_3, but does not appear in the CBP-spectrum[26] and a small shift in the Plasmon peak positions,[26] which are 23.06 eV and 23.14 eV for CBP and MoO_3, respectively. The peak position difference is smaller as for the experimentally obtained spectra of the neat films since in the composite MoO_3 is always embedded in the CBP matrix, leading to a mixed signal from both species. Moreover it is possible that the small MoO_3 agglomerates with sizes around 1 nm exhibit a different plasmon excitation energy than the bulk layer of pure MoO_3. The classification map for the doped sample is shown in Figure 3b, where MoO_3 is depicted in white and CBP in black. The comparison of this map with the zero-loss image in Figure 3a again shows a correlation. So we conclude that both bright field and spectroscopic images indicate that MoO_3 agglomerates in the CBP matrix for both doping concentrations.

2.3. Three-Dimensional Microstructure: Electron Tomography

In a recent publication,[23] it is suggested that MoO_3 is incorporated as spherical clusters into an organic matrix. But one must consider, that from the measurements presented so far, no information on the 3D structure of the MoO_3 agglomerates can be obtained, since these images only reflect 2D projections of the analyzed sample volume. To gain information on the 3D structure of the MoO_3 agglomerations and its spatial distribution within the CBP thin film electron tomography was applied. For this purpose, the choice of the proper imaging technique is essential. Bright-field imaging shows true material contrast, as already demonstrated. Furthermore, negligible diffraction contrast is observed, due to the amorphous nature of CBP as well as the MoO_3 agglomerates. Hence bright-field imaging satisfies the projection criterion in this special case and is thus capable as imaging technique for tomography. For tomographic reconstruction, a single axis tilt series consisting of zero-loss filtered bright-field images taken at tilt angles between −60° and 60° was acquired. A tilt angle incrimination scheme as proposed by Saxton et al.[31] (starting from $\Delta\alpha = 1°$ at $\alpha = 0°$ sample tilt) was applied. A movie with the full tilt series can be found in the Supporting Information (Movie 2). For image alignment and to take potential film deformations into account, gold fiducials were deposited onto both sides of the MoO_3-doped CBP film (see Experimental Section for more details). The acquired tilt series provided projections of the sample at different angles, from which a 3D volume was reconstructed using the IMOD software package[32] with the weighted back projection algorithm.[33,34] The reconstructed volume is shown in **Figure 4**, a

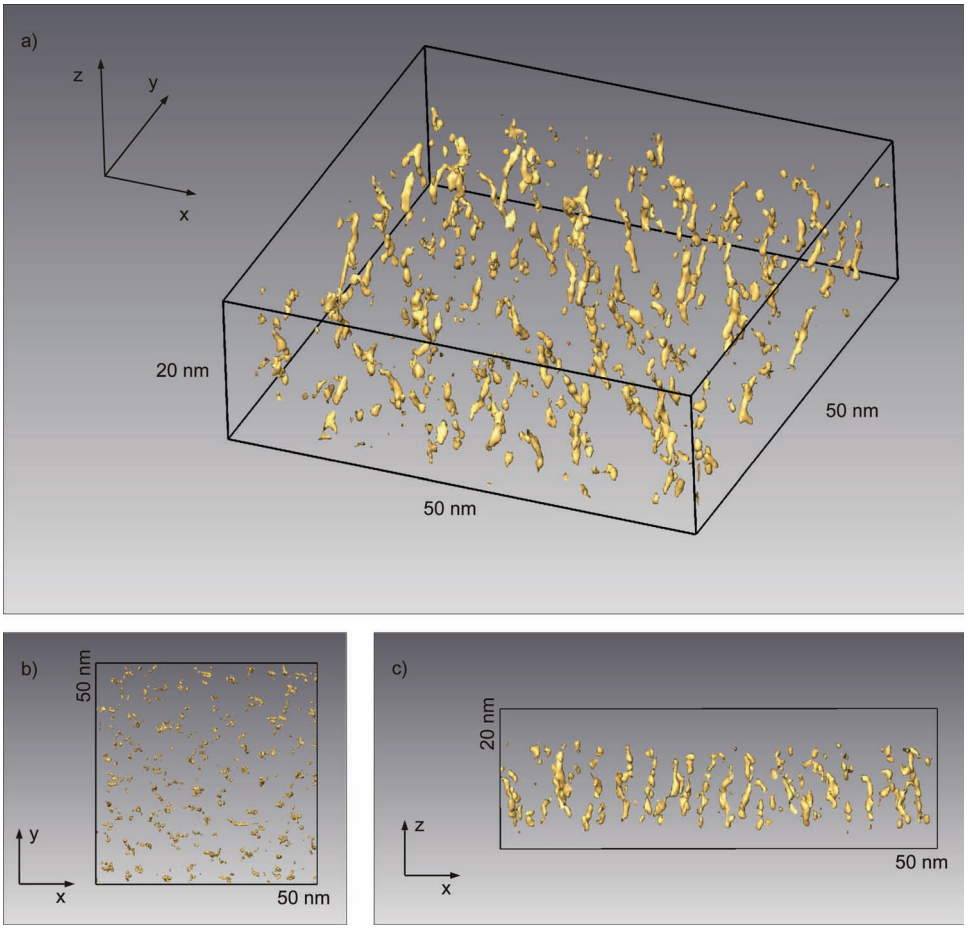

Figure 4. a) Segmentation in 3D of a reconstructed volume of MoO_3:CBP obtained from electron tomography for the sample with 10 vol% doping concentration. b) Top-view of *xy*-plane. c) Side-view of *xz*-plane.

movie of the reconstruction is shown in the Supporting Information (Movie 3). We observe, that MoO_3 when co-deposited with CBP, forms 1D nanostructures, best described by the term nanofilaments. These nanofilaments are preferentially oriented along the growth direction of the thin film. Figure 4b shows the reconstructed volume in a top view, which is remarkably similar to the bright-field projection images under perpendicular beam incidence (see Figure 1a). In an additional experiment, we deposited a multilayered film structure of the type CBP: MoO_3/CBP/CBP: MoO_3. Via electron tomography, we observed nanofilamentous growth of MoO_3 in the top and the bottom layer (see Supporting Information Figure S2). Due to the intrinsic CBP layer, which separates the two doped layers, the nanofilaments of top and bottom film appear to be uncorrelated.

2.4. Influence of Substrate Temperature on Filament-Growth

To gain information on the growth process we prepared a sample with 10 vol% doping concentration on a substrate cooled down to approximately 120 K during the evaporation process. A comparison of TEM images of a sample grown at room temperature and a sample grown at 120 K is seen in **Figure 5**a,b. A first striking difference is, that the apparent agglomeration of MoO_3 in the case of room temperature growth cannot be observed for samples grown at the lower temperature. To confirm, that comparable amounts of MoO_3 are present in both films, EELS spectra of both films were taken and are presented in Figure 5c. Compared to the neat MoO_3 film, the same characteristic loss features can be identified in both spectra of the doped films. As in Figure 2c the spectra are background-corrected and normalized with respect to the intensity of the peak at 532 eV. Since both spectra show comparable peak intensities at the oxygen K-edge, it can be concluded that both films contain similar amounts of MoO_3. Taking the instruments absolute resolution of 2 Å into account and considering low contrast ratios due the disordered film structure, we estimate that no particles of 10 Å or larger are present in the film. Berkowitz et al. found that for thermal evaporation of MoO_3 the vapor mainly consists of Mo_3O_9 molecules.[35] To form larger aggregates, the agglomeration process must take place on the surface of the sample. It can be deduced from our results that the growth-process leading to the observed agglomeration of MoO_3 must be diffusion limited. When depositing onto substrates at lower temperatures, the heat of the adsorbed MoO_3 species is quickly dissipated into the substrate, which limits the diffusion length and therefore the possibility of the MoO_3 molecules to interact with other MoO_3 species on the surface. This suppresses agglomeration of MoO_3 and hence no clusters can be observed within the resolution limit of our experiment. This is also supported by Lee et al.[23] who found a log-normal size distribution of MoO_3 clusters, which indicates a diffusion process on the substrate. The reason for the agglomeration can most probably be found in the very high surface energy of MoO_3 and therefore has a tendency to decrease its surface. Another factor, which could account for the agglomeration could be that the MoO_3 is accumulated at domain boundaries of CBP nanocrystals as packing for the molecules to maximize π-orbital overlap might be energetically favorable.

2.5. Charge Transport Along MoO_3-Filaments

P-doping of organic thin films to enhance the conductivity of these films and ultimately also device performance is one application, where transition metal oxides (e.g., MoO_3) are co-evaporated with organic molecules and which might be affected by the observed MoO_3 agglomeration. It is known from UPS measurements, that the ionization energy of CBP is lower than the electron affinity of MoO_3, which will enable electron transfer from CBP to MoO_3. This charge transfer was confirmed by FT-IR measurements.[36] In n- or p-doped organic thin films, charge transfer between the dopant species and the host molecules is essential to increase the conductivity of respective films,[19] and to improve device performance.[37–40] Although, in several previous publications on p-doping of organic thin films with MoO_3, an increased conductivity was described, doping efficiency was much lower than expected from purely energetic considerations. In this context, doping efficiency describes the ratio between targeted dopant density and measured carrier density. For MoO_3-doping, doping efficiencies in the range of 1% or even below are determined.[20,21,41] Previous interpretations of increased conductivity in MoO_3-doped organic thin films state that there are either homogenously dispersed acceptor molecules or small spherical clusters present in the film, which lead to an enhanced charge carrier density within the CBP matrix.

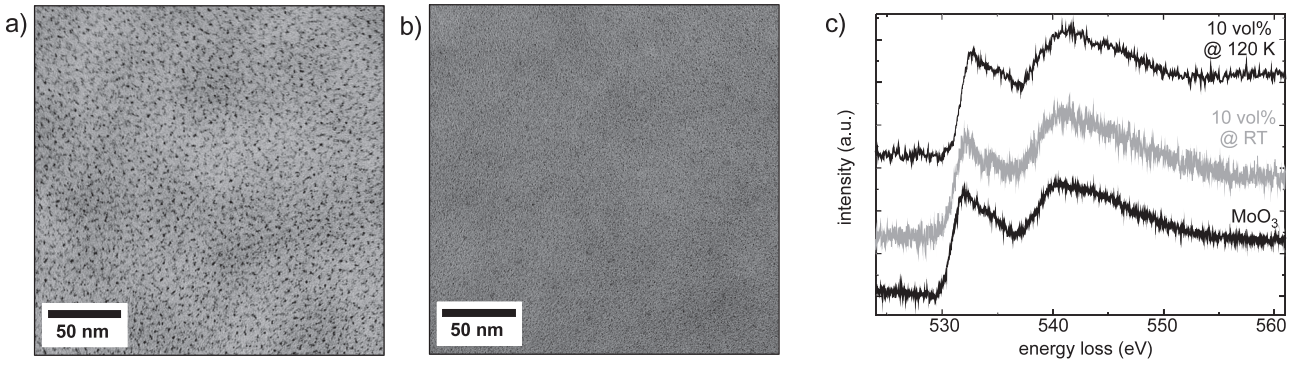

Figure 5. Bright-field images of a sample grown on a) substrate at room temperature and b) at 120 K. c) EELS-spectra of doped films grown on substrates at different temperatures and a neat MoO_3 film.

Considering now, that in mentioned publications vertical devices were under investigation,[19] and our findings indicate the presence of vertically aligned MoO_3 nanofilaments in such films, the reason for the increased conductivity must be much different than expected before. The observed charge transfer will occur at the interface between the MoO_3 nanofilaments and individual CBP molecules. This charge transfer will leave hole carriers on CBP molecules and increases the free electron density within the MoO_3 nanofilaments. Therefore, charge is most likely conducted at the surface of or within the vertically aligned filaments resulting in 1D conduction paths. Hence a highly anisotropic conductivity of co-evaporated MoO_3/CBP thin films is expected. Yet it is still unclear, whether the current is dominated by holes going through the CBP matrix or electrons being conducted via the MoO_3 nanofilaments. Generalizing, it can be expected that other dopants may behave similar. Furthermore, morphology effects should always be considered and checked, when discussing doping issues in organic thin films or devices based thereof. It was shown above, that the filament growth was suppressed at low temperatures, which we attribute to a drastically reduced diffusion of MoO_3 species on the surface of the sample during evaporation. Infrared spectroscopy can be used to determine the ratio of charged CBP molecules per number of dopants and can be taken as a quantitative indicator for how the morphology affects the density of charge carriers in doped films. There it was confirmed, that for deposition onto cooled substrates, the number of charged CBP molecules per Mo_3O_9-unit was increased by a factor of 1.8 compared to a sample grown at room temperature.[36] By molecular design and choosing the right growth temperature, it should be possible to tune the surface properties to either suppress or enable filament growth in co-evaporated organic/inorganic composites also for other inorganic materials. One instance can be nanofilamentous thermoelectric materials with 1D conductions paths of a few nanometers in width, which are expected to show a largely increased figure of merit as described in the literature.[7]

3. Conclusions

In conclusion, bright-field TEM images in correlation with ESI provide the information that MoO_3 has a strong tendency to form nanoclusters when co-deposited with organic materials such as CBP. Using electron tomography we observed that MoO_3 forms filament-like structures, which are preferentially oriented along the growth direction of the thin film. Furthermore we demonstrated that the agglomeration process can be suppressed by cooling down the substrate during the evaporation, hence this process must be diffusion limited. Our findings suggest, that in the specific case of MoO_3 being used as p-dopant in CBP, the MoO_3 filaments serve as 1D conductive paths. Numerical simulations will be carried out for further understanding which process is the driving force for the observed nanofilament formation and how to control it by other means than growth temperature manipulation. With this understanding nanofilament growth of further inorganic materials in tailored organic matrices will be within reach, which will have a major impact on numerous applications relying on controlled nanocomposites, such as thermoelectric devices.

4. Experimental Section

Materials and Sample Preparation: CBP (sublimed grade, 99.9% purity) and MoO_3 (99.99% purity) were obtained from Sigma Aldrich, poly(3,4-ethylenedioxythiophene):poly-(styrenesulfonate) (PEDOT:PSS; Clevios P VPAI 4083) was purchased from Heraeus Precious Metals. For sample preparation PEDOT:PSS was spin-coated on indium tin oxide (ITO)-coated borofloat glass with 2500 rpm. This interlayer allows for floating off the organic thin films, which were deposited by thermal evaporation in an integrated ultrahigh vacuum (UHV)-system at a base pressure of 10^{-8} mbar. Doped films were prepared by co-evaporation of the single materials. Deposition rates for the neat films were 50 Å/min. For the doped samples CBP was evaporated at about 50 Å/min and the MoO_3-rate was accordingly adapted to achieve the respective doping concentration. Film thicknesses were monitored by oscillating quartz-crystals. The thin films were then floated in demineralized water and picked up with holey carbon grids (Quantifoil). Because for MoO_3 the floating process did not work, a sample with 70 nm MoO_3 and a 20 nm thick CBP-film as supporting layer was prepared for the core-loss spectra. Since CBP does not contain oxygen the corresponding EELS-spectra only contain signal from the MoO_3-film. Low-loss EELS-spectra for neat CBP and MoO_3 films were both recorded with Quantifoil-background for better comparability. For electron tomography, gold nanoparticles where dispersed on the front and back side of the samples as fiducials. The gold nanoparticle solution was purchased from Aurion and mixed with deionized water at a 1:1 concentration. To ensure a homogeneous dispersion of gold nanoparticles on the surface of the samples, samples were treated for 6 s (Gatan Solarus (Model 950) Advanced Plasma Cleaning System) with 50 W oxygen plasma before applying the fiducials. Acquiring a bright-field image before and after the plasma-treatment showed no occurring structural changes of the thin films due to the treatment.

Microscopy: All measurements were performed with a Libra 200 MC Cryo DMU (Carl Zeiss Microscopy), which provides high spatial resolution as well as high energy resolution due to the combination of a monochromater and an in-column energy filter. Low-loss ESI measurements were performed with 60 kV acceleration voltage because of a higher cross-section as well as higher dispersion which leads to an improved energy resolution for the ESI data set. 200 kV was used for the core-loss spectroscopy measurements to diminish multiple scattering contributions to the spectral signal for detailed analysis.

Supporting Information

Supporting Information is available from the Wiley Online Library or from the author.

Acknowledgements

The authors thank T. Glaser and S. Beck (University of Heidelberg, Germany) for the preparation of the sample on the cooled substrate. Financial support by the German Federal Ministry for Education and Research (FKZ 13N10723 and FKZ 13N10794) is gratefully acknowledged.

Received: July 25, 2012
Revised: October 16, 2012
Published online: November 21, 2012

[1] D. Green, D. Walsh, S. Mann, R. O. C. Oreffo, *Bone* **2002**, *30*, 810.
[2] S. Lal, S. Link, N. J. Halas, *Nat. Photonics* **2007**, *1*, 641.
[3] C. Lee, I. Kim, W. Choi, H. Shin, J. Cho, *Langmuir* **2009**, *25*, 4274.
[4] S. K. Hwang, J. M. Lee, S. Kim, J. S. Park, H. I. Park, C. W. Ahn, K. J. Lee, T. Lee, S. O. Kim, *Nano Lett.* **2012**, *12*, 2217.

[5] J. J. M. Halls, C. A. Walsh, N. C. Greenham, E. A. Marseglia, R. H. Friend, S. C. Moratti, A. B. Holmes, *Nature* **1995**, *376*, 498.
[6] M. S. Dresselhaus, G. Chen, M. Y. Tang, R. Yang, H. Lee, D. Wang, Z. Ren, J.-P. Fleurial, P. Gogna, *Adv. Mater.* **2007**, *19*, 1043.
[7] L. D. Hicks, M. S. Dresselhaus, *Phys. Rev. B* **1993**, *47*, 16631.
[8] M. Li, B. Lebeau, S. Mann, *Adv. Mater.* **2003**, *15*, 2032.
[9] J. D. Hopwood, S. Mann, *Chem. Mater.* **1997**, *9*, 1819.
[10] D. Pradhan, M. Sharon, *Mater. Sci. Eng.: B* **2002**, *96*, 24.
[11] D. J. Cott, N. Petkov, M. A. Morris, B. Platschek, T. Bein, J. D. Holmes, *J. Am. Chem. Soc.* **2006**, *128*, 3920.
[12] S. H. Park, A. Roy, S. Beaupré, S. Cho, N. Coates, J. S. Moon, D. Moses, M. Leclerc, K. Lee, A. J. Heeger, *Nat. Photonics* **2009**, *3*, 297.
[13] P. Peumans, S. Uchida, S. R. Forrest, *Nature* **2003**, *425*, 158.
[14] M. Pfannmöller, H. Flügge, G. Benner, I. Wacker, C. Sommer, M. Hanselmann, S. Schmale, H. Schmidt, F. A. Hamprecht, T. Rabe, W. Kowalsky, R. R. Schröder, *Nano Lett.* **2011**, *11*, 3099.
[15] M. A. Baldo, M. E. Thompson, S. R. Forrest, *Nature* **2000**, *403*, 750.
[16] G. J. McGraw, D. L. Peters, S. R. Forrest, *Appl. Phys. Lett.* **2011**, *98*, 013302.
[17] J. Meyer, S. Hamwi, S. Schmale, T. Winkler, H.-H. Johannes, T. Riedl, W. Kowalsky, *J. Mater. Chem.* **2009**, *19*, 702.
[18] W.-Y. Wong, G.-J. Zhou, X.-M. Yu, H.-S. Kwok, Z. Lin, *Adv. Funct. Mater.* **2007**, *17*, 315.
[19] M. Kröger, S. Hamwi, J. Meyer, T. Riedl, W. Kowalsky, A. Kahn, *Org. Electron.* **2009**, *10*, 932.
[20] S. Hamwi, J. Meyer, T. Winkler, T. Riedl, W. Kowalsky, *Appl. Phys. Lett.* **2009**, *94*, 253307.
[21] M. Lehnhardt, S. Hamwi, M. Hoping, J. Reinker, T. Riedl, W. Kowalsky, *Appl. Phys. Lett.* **2010**, *96*, 193301.
[22] W. Ma, C. Yang, A. Heeger, *J. Adv. Mater.* **2007**, *19*, 1387.
[23] J.-H. Lee, H.-M. Kim, K.-B. Kim, J.-J. Kim, *Org. Electron.* **2011**, *12*, 950.
[24] R. F. Egerton, *Rep. Prog. Phys.* **2009**, *72*, 016502.
[25] R. Egerton, M. Malac, *J. Electron Spectrosc. Relat. Phenom.* **2005**, *143*, 43.
[26] L. Reimer, U. Zepke, J. Moesch, S. Schulze-Hillert, M. Ross-Messmer, W. Probst, E. Weimer, *EELS-Spectroscopy: a Reference Handbook of Standard Data for Identification and Interpretation of Electron Energy Loss Spectra and for Generation of Electron Spectroscopic Images*, Carl Zeiss, Electron Optics Division, Oberkochen **1992**.
[27] D. Wang, D. S. Su, R. Z. Schlögl, *Anorg. Allg. Chem.* **2004**, *630*, 1007.
[28] R. F. Egerton, *Electron Energy-Loss Spectroscopy in the Electron Microscope*, 2nd Ed., Springer, New York **1996**.
[29] D. B. Williams, C. B. Carter, *Transmission Electron Microscopy: A Textbook for Materials Science*, 2nd Ed., Springer, New York **2009**.
[30] L. Reimer, H. Kohl, *Transmission Electron Microscopy: Physics of Image Formation*, 5th Ed., Springer, New York **2008**.
[31] W. O. Saxton, W. Baumeister, M. Hahn, *Ultramicroscopy* **1984**, *13*, 57.
[32] J. R. Kremer, D. N. Mastronarde, J. R. McIntosh, *J. Struct. Biol.* **1996**, *116*, 71.
[33] I. Kazantsev, The weighted backprojection techniques of image reconstruction. In: Computer Analysis of Images and Patterns, *Lect. Notes Comput. Sci.* Springer, Berlin **1995**, *970*, p. 521–525.
[34] M. Radermacher, *Weighted Back-projection Methods. In: Electron Tomography: Three-Dimensional Imaging with the Transmission Electron Microscope (Mathematical Concepts and Methods in Science and Engineering)*, Plenum Press, New York **1992**, p. 91–115.
[35] J. Berkowitz, M. G. Inghram, W. A. Chupka, *J. Chem. Phys.* **1957**, *26*, 842.
[36] T. Glaser, S. Beck, B. Lunkenheimer, D. Donhauser, A. Köhn, M. Kröger, A. Pucci, *Org. Electron.* **2013**, *14*, 575.
[37] S. Hamwi, T. Riedl, W. Kowalsky, *Appl. Phys. Lett.* **2011**, *99*, 053301.
[38] D. Qin, J. Liu, Y. Chen, L. Chen, W. Quan, G. Li, *Semicond. Sci. Technol.* **2012**, *27*, 045012.
[39] G. Xie, Y. Meng, F. Wu, C. Tao, D. Zhang, M. Liu, Q. Xue, W. Chen, Y. Zhao, *Appl. Phys. Lett.* **2008**, *92*, 093305.
[40] K. Walzer, B. Maennig, M. Pfeiffer, K. Leo, *Chem. Rev.* **2007**, *107*, 1233.
[41] J.-H. Lee, D.-S. Leem, H.-J. Kim, J.-J. Kim, *Appl. Phys. Lett.* **2009**, *94*, 123306.